Eidgenössische Technische Hochschule Zürich
Swiss Federal Institute of Technology Zurich

The Measurement of Positronium 1S-2S Spectroscopy

Summer Thesis

Yifeng Wang

wang3128@purdue.edu

Laboratory for Positron and Positronium Physics
Department of Physics | Institute for Particle Physics and Astrophysics
ETH Zürich

Supervisors:
Dr. Paolo Crivelli, Michael Heiss

November 23, 2019

Acknowledgements

I would like to thank Dr. Crivelli for giving me the chance to work in this positronium lab during summer and coordinate relevant issues. Also, his advise in the data analysis part was very valuable and insightful. Then, I would like to thank Prof. Dissetori; he interviewed me before I came to ETH and contacted Dr. Crivelli to make this summer research possible.

For the trap and buncher part, I worked mostly with Michael. I want to thank him for his patient explanation of the theoretical background and relevant engineering problem, which is very crucial to this report. Beyond physics, his versatility in electrical, mechanical, and computer fields enriched my research experience. I want to thank Lars for giving me help on MATLAB simulation. I also want to thank Zakary for advising me on writing report and providing me with reference resources.

Abstract

The thesis is meant to report on my contribution to the research work conducted within the positronium group at ETH. The goal of this experiment is to measure with high precision of energy of the 1S-2S excitation of positronium, which can either correct the recent experimental results of 2 sigmas away from the theory or confirm the discrepancy between experiment and theory with higher confidence, namely 0.5 ppm [1]. The Second-Order Doppler Effect and Stark Effect are calculated and considered based on the experiment setup [2].

The experimental apparatus consists of a Na^{22} source of positron, a rotating magnetic trap, a voltage gate to control the release of positron, a buncher for time compression of positron beam, an elevator to accelerate the beam, a silicon target that diffuses positronium out after bombarded by the beam, a laser apparatus to excite 1S to 2S and a MCT (multiple channel plate) for detecting 2S as *signal*.

First, the trap, buncher, and elevator were adjusted for optimization so that the 50ns positron beam from the gate is compressed to a desired length of 15ns. I wrote a simulation of positrons' energy and time spread at each critical position between the gate and the target. This software is used as the guidance for optimization.

Second, the data were analyzed to extract the 2S positrons annihilation signal from the background and build the line-shape of the laser spectroscopy. Moreover, it is possible to conduct the other 2S-20P measurement with the same setup with only an additional laser for creating that transition [3].

The beam was bunched to about 15 ns when the thesis was finished and is still being improving by adjusting the bunch waveform. The data collected back then does not clearly indicate a presence of *signal*, i.e., the laser-on datasets do not have statistically more events than laser-off datasets. The reasons can be the beam length was not desirable at that time, the MCP does not have spatial resolution to distinguish the excess of 2S and other miscellaneous mis-adjustment can compromise the production and detection of the 2S. However, the MATLAB simulation can make the future adjustment controllable and the decay time in Tab. 6.1 indicates a significant shortening in positron beam length.

Contents

Chapter 1

Introduction

The study of purely leptonic system, which consists of a particle and its anti-particle in a bounded two-body system, can be treated back to 1934. Mohorovicic proposed the Positronium (Ps), i.e. an electron and a positron, in theory. Then, Deutsch detected Ps experimentally in 1951 [4]. This leptonic system is advantageous in precise measurement of fine structure constant, because for any two-body system the energy level and Rydberg constant is related as

$$E_i = -\frac{R_\infty hc}{n_i^2}\frac{1+\delta_i}{1+m_1/m_2}, \tag{1.1}$$

where n_i is the principle quantum number and δ_i is the theoretical correction; the determination of different energy levels can lead to a close calculation of Rydberg constant only limited by the knowledge of small theoretical correction corresponding to each level used [5]. Also, Rydberg constant contains the fine structure constant.

$$R_\infty = \frac{m_e e^4}{8\epsilon_0^2 h^3 c} = \frac{m_e c}{2h}\left(\frac{1}{4\pi\epsilon_0}\frac{e^2}{\hbar c}\right)^2 = \frac{m_e c}{2h}\alpha^2. \tag{1.2}$$

The infinite sign indicates it is the Rydberg constant that assumes an infinite mass of one particle, i.e. a hydrogen atom with proton having infinite mass, thus the reduced mass is just m_e. Similarly, Rydberg constant for a positronium system is one-half of that of infinity, because the reduced mass is given by $\frac{m_{e^+}m_{e^-}}{m_{e^+}+m_{e^-}} = \frac{m_e}{2}$.

Because the uncertainty of the finite nuclear size of the proton from QCD, the best hydrogen 1s-2s transition only reached a precision of 4.2 ppb [6]. For Ps, without the "finite size" problem, we can measure the energy of any two level of transition to get the Rydberg constant and then fine structure constant. In this experiment, the 1s-2s transition is chosen. We determine the energy difference of 1s-2s of Ps by detuning the laser frequency to search for the laser energy that makes the most 1s-2s transition. The excess 2s is detected by a MCP.

Chapter 2

Theoretical background for 1S-2S excitation of Ps

The positronium (e^+e^-, Ps) and muonium (μ^+e^-, M) as the purely leptonic system are the ideal tools for testing especially the higher-order correction in QED, comparing to hadronic particles, like a hydrogen atom, that is subject to finite-size effects. The experiments on those bounded leptonic systems can be used to test CP violation and even beyond the Standard-Model. The 1S-2S transition of positronium was first studied in 1982 [7]. The idea was shooting positrons to silica powders and make them captured by electrons, such that bound-state particle, Ps, is then excited by a laser with specific frequency to 2S. Measuring such frequency (energy) of the laser is a sensitive probe for Standard-Model Extension. By far, all relevant measurements are within QED calculations for 5 sigma significance.

2.1 Lorentzian line profile

In the spectra of atom, spectral lines are always not strictly monotonic, because of the uncertainty principle, which states that change in energy cannot be infinitely small given the time of observation is finite. Indeed, the spectra distribution $I(v)$ of absorbing or emission frequency of atom form a Lorentzian shape around the center frequency $v_0 = (E_i - E_k)/h$, where E_i and E_k are the energy of two levels of transition. The line shape corresponding to the spreads of E_i and E_k can be studied as a classic damped oscillator with frequency w, mass m, restoring force k and damping constant γ. By solving the differential equation

$$\ddot{x} + \gamma\dot{x} + \omega_0^2 x = 0, \tag{2.1}$$

one can obtain the approximate amplitude

$$x(t) \approx x_0 e^{-(\gamma/2)t} \cos(\omega_0 t) \tag{2.2}$$

with the assumption of small damping ($\gamma \ll \omega_0$) [8]. By applying the unilateral Fourier transform

$$A(\omega) = \frac{1}{\sqrt{2\pi}} \int_0^\infty x_0 e^{-(\gamma/2)t} \cos(\omega_0 t) e^{-i\omega t} \mathrm{d}t \tag{2.3}$$

which is the frequency domain. The lower integration limit must be 0 because $x(t) = 0$ for $t < 0$. Thus, the equation above then is solved as

$$A(\omega) = \frac{x_0}{\sqrt{8\pi}} \left(\frac{1}{i(\omega - \omega_0) + \gamma/2} + \frac{1}{i(\omega + \omega_0) + \gamma/2} \right). \tag{2.4}$$

Close to central frequency ω_0, where $(\omega - \omega_0)^2 \ll \omega_0^2$, so one term is negligible and the intensity profile of the spectral line is

$$I(\omega - \omega_0) = \frac{C}{(\omega + \omega_0) + (\gamma/2)^2}, \tag{2.5}$$

where $C = I_0 \gamma / 2\pi$. The normalized Lorentzian profile is

$$L(\omega - \omega_0) = \frac{\gamma/2\pi}{(\omega + \omega_0) + (\gamma/2)^2}. \tag{2.6}$$

To note, the full halfwidth at half-maximum (FWHM) is

$$\delta\omega_n = \gamma \quad \text{or} \quad \delta\nu_n = \gamma/2\pi = \Gamma/\pi. \tag{2.7}$$

2.2 Lifetime

The lifetime of exotic atom can be obtained by rearranging (2.1) to solve for the radiant power, which yields

$$\frac{\mathrm{d}W}{\mathrm{d}t} = P = -\gamma m x_0^2 \omega_0^2 e^{-\gamma t} \sin^2 \omega_0 t. \tag{2.8}$$

As the time average $\overline{\sin^2 \omega t} = 1/2$, the time-averaged radiant power is

$$\overline{\frac{\mathrm{d}W}{\mathrm{d}t}} = \overline{P} = -\frac{\gamma}{2} m x_0^2 \omega_0^2 e^{-\gamma t}, \tag{2.9}$$

which shows the the intensity I has the decay time of $\tau = 1/\gamma$. If taking into account of all the decay channels, Einstein coefficient A_i should be introduced to replace the damping coefficient γ as a more formal description of the frequency distribution of spontaneous emission corresponding to the lineshape. As stated in the uncertainty principle, $\Delta E_i \simeq \hbar/\tau_i$, so the average lifetime τ_i of a specific excited level of energy E_i is given by

$$\delta\omega = \Delta E_i / \hbar = 1/\tau_i, \tag{2.10}$$

which in the case of this experiment is enough, because 1S is the ground state that the energy E_k do not contribute its uncertainty to the linewidth.

Specifically, the lifetime of Ps depends which Zeeman sublevels the positron and electron are on. For 1S, the ortho-Ps lifetime is 142 ns and the para-Ps is less than 1 ns. For 2S, the ortho-Ps lifetime is 1.1 μs and the para-Ps is 144 ns. In this experiment of exciting 1S to 2S, most Ps are in the ortho spin configuration, because Ps reach the MCP after excitation in 400 ns; most para-Ps should decay to photons before reach MCP. Therefore, only ortho-Ps annihilation should be detected as signal by MCP.

Another prominent value to measure precisely is the lifetime of the ortho-Ps at 1S, which can be done with almost the same experiment set-up. With the precisely measurement of 1S decay time and some corrections, its HFS can be obtained.

2.3 AC Stark effect

In this section and the following section, the two-body Coulomb system is studied with the assumption that the driving laser is monochromatic and no three-photon transition happens to the ground state Ps. Due to the selection rule, 1s-2s transition cannot be single-photon, as $|\Delta l| = 0$. Consider the classic time-dependent Hamiltonian of a Ps

$$H(t) = \hat{H}_0 + V(t), \tag{2.11}$$

where

$$\hat{H}_0 = \frac{\boldsymbol{P}^2}{m_e} - \frac{K_e e^2}{2r}, \tag{2.12}$$

$$\begin{aligned} V(t) &= V\frac{1}{2}[\exp(i\omega_L t) + \exp(-i\omega_L t)], \\ V &= -e\epsilon_L \hat{\boldsymbol{z}}. \end{aligned} \tag{2.13}$$

The V is an incident plane wave field and the dipole approximation is made for the interaction Hamiltonian. The wavefunction can be expressed as a superposition of the ground and excited states as

$$|\Psi(t)\rangle = c_g(t)\exp(-i\omega_g t)\,|g\rangle + c_e(t)\exp(-i\omega_e t)\,|e\rangle\,. \tag{2.14}$$

The solution to its Schrödinger equation is

$$\begin{aligned} \dot{c}_g &= i\frac{\Omega^*}{2}\exp(-i\Delta t)c_e(t), \\ \dot{c}_e &= i\frac{\Omega}{2}\exp(i\Delta t)c_g(t), \end{aligned} \tag{2.15}$$

where $|c_g|^2$ and $|c_e|^2$ represent the percentage of the population in the ground and excited state, respectively, and $|c_g|^2+|c_e|^2=1$. Thus, we can define two new coefficients to replace them without changing physical meaning of the system as

$$\begin{aligned} c_g^{'}(t) &= c_g(t), \\ c_e^{'}(t) &= c_e(t)\exp(i\Delta t). \end{aligned} \tag{2.16}$$

Besides, the time derivative of these new defined coefficients become

$$\begin{aligned} i\hbar\dot{c_g^{'}}(t) &= \frac{\hbar\Omega}{2}c_e^{'}(t), \\ i\hbar\dot{c_e^{'}}(t) &= \frac{\hbar\Omega}{2}c_g^{'}(t) - \hbar\Delta c_e^{'}(t). \end{aligned} \tag{2.17}$$

The resonant Rabi frequency Ω for the system close to resonance $(\omega_l+\omega_a) \gg \Delta$ and frequency detuning Δ is defined as

$$\Omega = \frac{\langle e|\hat{\boldsymbol{z}}|g\rangle \cdot \vec{E}_0}{\hbar} = 2(2\pi\beta_{ge})I \qquad \Delta = \omega_l - \omega_a, \tag{2.18}$$

and the intensity of the plane wave is defined as

$$I = \frac{1}{2}\epsilon_0 c\mathcal{E}_L^2. \tag{2.19}$$

For the sake of matching with the density matrix formalism, density operator ρ is introduced as

$$\rho = |\Psi\rangle\langle\Psi|, \tag{2.20}$$

so that ρ and c_i can be related through

$$\rho_{ge} = \langle g|\rho|e\rangle = \langle g|\Psi\rangle\langle\Psi|e\rangle = c_g c_e^*. \tag{2.21}$$

Therefore, for the two level system the density matrix is given simply as

$$\rho = \begin{pmatrix} \rho_{ee} & \rho_{eg} \\ \rho_{ge} & \rho_{gg} \end{pmatrix}, \tag{2.22}$$

thus gives the correct physical meaning of the two system populations in ground and excited state, as $\rho_{ee}+\rho_{gg}=1$ and ρ_{eg} and ρ_{ge} represent the coherences between these two states. From this matrix formalism the spontaneous emission can be described as an exponential decay of the coherences at a constant rate, like

$$\left(\frac{\mathrm{d}\rho_{eg}}{\mathrm{d}t}\right)_{spon} = -\frac{\Gamma}{2}\rho_{eg}, \tag{2.23}$$

where Γ is the lifetime of the excited state. From here, Optical Bloch Equations can be derived as

$$\begin{aligned}
\dot{\rho}_{gg} &= \Gamma\rho_{ee} - \frac{i\Omega}{2}(\rho_{eg} - \rho ge) \\
\dot{\rho}_{ee} &= -\Gamma\rho_{ee} + \frac{i\Omega}{2}(\rho_{eg} - \rho_{ge}) \\
\dot{\rho}_{eg} &= (i\delta - \frac{\Gamma}{2})\rho_{eg} + \frac{i\Omega}{2}(\rho_{ee} - \rho_{gg}) \\
\dot{\rho}_{eg} &= (-i\delta - \frac{\Gamma}{2})\rho_{ge} - \frac{i\Omega}{2}(\rho_{ee} - \rho_{gg}).
\end{aligned} \tag{2.24}$$

Then, population difference can be defined as $\omega = \rho_{gg} - \rho_{ee} = 1 - 2\rho_{ee}$, thus

$$\frac{\mathrm{d}\omega}{\mathrm{d}t} = \frac{\mathrm{d}\rho_{gg}}{\mathrm{d}t} - \frac{\mathrm{d}\rho_{ee}}{\mathrm{d}t} = \Gamma(1-\omega) - i\Omega(\rho_{eg} - \rho_{ge}); \tag{2.25}$$

consequently,

$$\dot{\rho}_{eg} = (i\delta - \frac{\Gamma}{2})\rho_{eg} + \frac{i\omega\Omega}{2}. \tag{2.26}$$

For the perturbation potential in steady-state, $\dot{\omega} = \dot{\rho}_{eg} = 0$. Therefore, we can conclude

$$\begin{aligned}
\omega &= \frac{1}{1+s} \\
\rho_{eg} &= \frac{i\Omega}{2(\Gamma/2 - i\delta)(1+s)},
\end{aligned} \tag{2.27}$$

where $s = \frac{|\Omega|^2}{2|\Gamma/2 - i\delta|^2} = \frac{\Omega^2/2}{\delta^2 + \Gamma^2/4} = \frac{s_o}{1+(2\delta/\Gamma)^2}$ is the saturation parameter which indicates the degree of the system is saturated for the excited state.

For the case of our experiment, the two-photon transition matrix elements can be calculated by adding sing-photon transition matrix elements with a known second-order perturbation $H^{(2)}$. One of the time-dependent two-photon transition matrix element is

$$\begin{aligned}
\beta_{ge} &= \left\langle e \middle| V(t) \frac{1}{(E_g + \hbar\omega_L) - H_0} V(t) \middle| g \right\rangle \\
&= -\frac{e^2}{2hc\epsilon_0} \left\langle e \middle| z \frac{1}{H_0 - (E_g + \omega_l)} z \middle| g \right\rangle,
\end{aligned} \tag{2.28}$$

where E_g is just the energy of the ground state given by

$$E_g = -\frac{(Z\alpha)^2 m_e c^2}{2n^2}, \tag{2.29}$$

with α being the fine-structure constant. From 2.14 the Hamiltonian of this two-level H can be obtained as

$$H = E_g|g\rangle\langle g| + E_e|e\rangle\langle e| + \frac{\hbar\Omega}{2}[\exp(i\omega_L t) + \exp(-i\omega_L t)]^2 \cdot (|e\rangle\langle g| + |g\rangle\langle e|), \tag{2.30}$$

with the eigenvalue of each state defined as

$$\begin{aligned} E_g &= h\nu_g + h\Delta\nu_{ac}(g), \\ E_e &= h\nu_e + h\Delta\nu_{ac}(e). \end{aligned} \tag{2.31}$$

The frequency shift $\Delta\nu_{ac}$ is defined by

$$\Delta\nu_{ac} = \beta_{ac} I(t), \tag{2.32}$$

where β_{ac} is the ac stark shift coefficient. The detailed calculation is described in [2], for hydrogen. Therefore, to calculate it specific for positronium it must be multiplied by a factor

$$\frac{1}{Z^4}\left(\frac{m_e}{\mu}\right)^3 = 8, \tag{2.33}$$

where μ is the reduced mass for positronium which is $m_e/2$ and Z is the nuclear charge.

Besides, I the intensity of laser, which has power of 1 kW and beam waist of 0.5 mm is estimated by

$$I = \frac{P}{\pi w^2/2} \approx 2.55 \times 10^9 \quad W/m^2 \tag{2.34}$$

Combine with Eq. 2.32, one can calculate the AC stark effect.

2.4 Doppler effect

In our experiment, the counter-propagating photons is used to excite the 1S positronium. The two-photon absorption can be described by a two-step process that goes from $|i\rangle$ through a virtual intermediate state $|v\rangle$ to the final state $|f\rangle$, thus by introducing a virtual state the probability amplitude from $|i\rangle \to |f\rangle$ is equivalent to the sum of probability amplitude of $|i\rangle \to |v\rangle$ and $|k\rangle \to |f\rangle$ with the detuning frequency of $\omega - \omega_{ik}$ and $\omega - \omega_{kf}$ respectively.

We can modify the derived Lorentz-line profile in Eq. 2.6 to show the probability of transition as

$$\begin{aligned} A(\omega) = C\Delta N^0 I^2 &\left| \sum_m \frac{(\boldsymbol{D}_{im}\hat{\boldsymbol{e}})(\boldsymbol{D}_{mf}\hat{\boldsymbol{e}})}{\omega - \omega_{im}} \right|^2 \\ &\times \left(\exp\left[-\left(\frac{\omega_{if} - 2\omega}{2kv_p} \right)^2 \right] + \frac{kv_p}{\sqrt{\pi}} \frac{\gamma_{if}/2}{(\omega_{if} - 2\omega)^2 + (\gamma_{if}/2)^2} \right), \end{aligned} \tag{2.35}$$

where C is a normalization constant, ΔN^0 is the non-saturated population difference, $\boldsymbol{D}$ is the matrix element of any transition and v_p is the most probable

velocity of the positronium. We can then expand the above equation to quantify the effect of different orders of Doppler shift.

To note, only second-order Doppler shift will be added to the systematic uncertainty for this experiment, while the first-order one does not count, because two counter-propagating photons set-up can eliminate its effect.

Chapter 3

The cyclotron buffer gas trap

A cyclotron trap is used to store the positrons produced by the process that $Na^{22} \rightarrow Ne^{22} + \beta^+ + \nu_e$. This process has a branching ratio Γ of 90.6% and endpoint energy T_{max} of 545 keV and the lifetime of Na^{22} is 2.6 years. Inside the trap, the energy of the positrons are reduced to less than 7 eV by the buffer gas. A rotating magnetic field of certain frequency is used to constrain the motion of positrons [9].

3.1 Principle of the cyclotron trap

With the continuous moderated beam intensity of 20000 e^+s^{-1} energy can be extracted from the positrons to trap them. A technique of rotating magnetic field is used to transfer the positron motion in the direction parallel to the field to perpendicular one. This technique is called "virtual trapping", because some positrons will be gradually lost as their motion are not in correct phase with magnetic field rotating [10]. Thus, buffer gas is also introduced to increase the trapping efficiency. The pressure of gas and electric potential of each stage are in descendent order, so that the positrons lose energy by passing through each stage, move on to next stage and eventually trapped in the last stage. A gate with potential higher than all stages is used to stop the positrons and scatter them back.

The energy distribution of the positrons still obeys the Boltzmann distribution, thus the energy spread is governed by the ambient temperature which is corresponding to the trapping gas. A cooling method could be used in the last stage to significantly decrease the energy spread positrons, which can simplify and improve the bunching part later.

3.2 Verification and optimization

The energy distribution function is measured by the technique of changing the gate voltage. For instance, when lowering the gate voltage for a short period of time (50 ns) positrons will be extracted from the trap as they have the energy estimated to be around 7 eV, and the number of positrons released are measured by a scintillator or a MCP. The result from the MCP is plotted in Fig. 3.1, which implies the voltage region (7.0 V to 8.0 V) of partial positrons passing through the gate reflect the energy spread of the positrons in the trap.

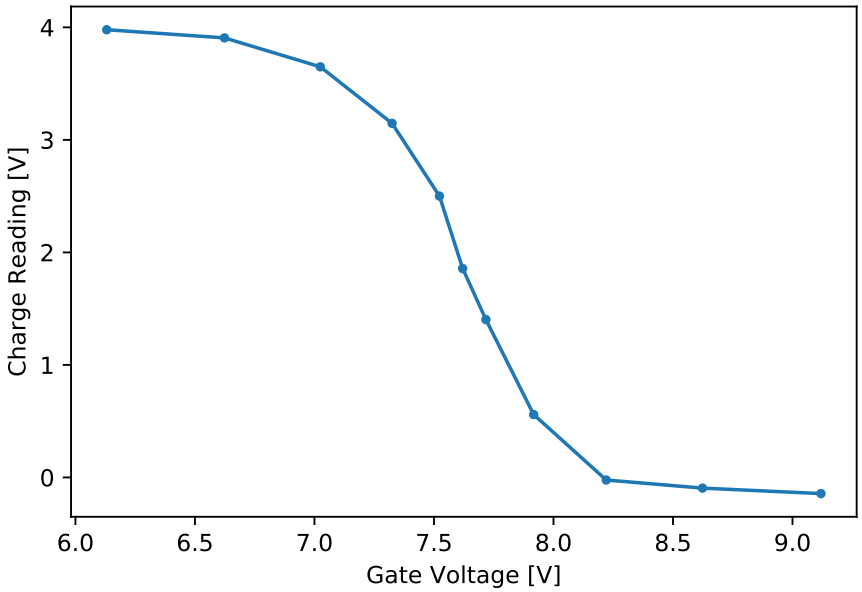

Figure 3.1: The measurement of the number of positrons pass through the gate w.r.t. the gate voltage

Therefore, differentiating charge reading with gate voltage can give the positron number at any specific energy [11]. Then, a skewed gaussian function is fitted to the data from which the mean μ and standard deviation σ can be infer statistically. The skewness is expected because Bolzmann distribution is skewed to lower energy.

Based on Fig. 3.2, a lower σ is desired for the trap for the next stage, the bunching, to work with high efficiency. The optimization of the rotating magnetic field frequency and gas pressure and voltage of each buffer stage is done by an automatic python script with a trial-and-error algorithm. By fixing all other parameters, scanning through the range of possible best value of one parameter the best value is obtained at this condition. Since the initial values are set based on

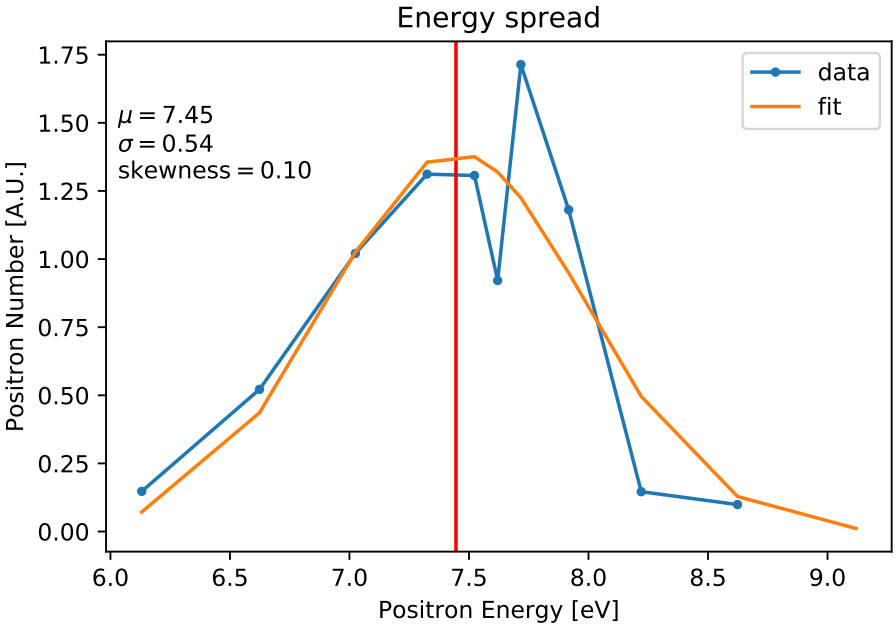

Figure 3.2: Differentiating of Fig. 3.1, the energy distribution of positrons is shown

theoretically calculated values, it is believed that this "multi-dimensional fitting" can be achieved within a reasonable number of iterations.

The σ was around 1.5 with old parameters and is improved to be 0.54 now. The energy spread is then interpolate to feed into the MATLAB simulation as the initial condition for the positron beam for Fig.4.2.

Chapter 4

Time compression of positron beam

A short metal tube less than 50 cm which can vary its potential very fast is used to change the energy of the positrons so that the beam length can be compressed to less than 10 ns FWHM when it reaches the target. After leaving the tube, the positrons will have gradient energy distribution with time such that latter ones will catch up earlier ones at the target.

4.1 Principle of the buncher

The buncher consists of a metal shield connected to an amplifier and a function generator. The voltage of the the buncher relative to the ground is given by the arbitrary waveform generator by the function generator and amplified by the amplifier. The energy of the positrons inside the buncher is assumed to be unchanged as they do not experience any electric force. The bunch time should be critically coupled to the gate to assure all positrons enter the buncher before the potential starts to change with arbitrary waveform. The voltage offset, shown in Fig. 4.3, can be chosen for the buncher to reduce the energy of the positrons. As the arbitrary waveform is limited by the amplifier rising speed, the time of flying must exceed the minimum time of rising of this set-up. When the positrons are all in the buncher and the first one starts to leave, the potential changes as

$$V_b(t) = V_0 + \frac{m_e l^2}{2q_e}(t_f - t)^{-2}, \tag{4.1}$$

where V_0 is the initial buncher potential relative to the ground, l represents the bunching length scale, and t_f is just a time offset [12]. This analytic solution is perfect for the ideal case, in which the positron beam is mono-energetic, and is verified by the MATLAB simulation program.

4.2 Simulation

An algorithm to convolute the energy distribution and time distribution at particular position with potential at that position is used to build the simulation software. When the positrons pass through a set point corresponding to each own time of arrival, the energy will be added or subtracted to each of them according to the buncher potential $V_b(t)$ and elevator potential $V_{el}(t)$. For example, varying the potential before the positrons start to leave the tube will not change their energy until they exit the tube; on the other hand, positrons leave at the same time will add the same energy implies the energy spread can degrade the bunching effect. This algorithm is the perfect analog to the real physics scenario and can be studied for the case of non-ideal case if the real initial time-energy distribution is inputed.

We first measured the time distribution of the positrons after the trap shown in Fig. 4.1. As the voltage change of the gate is not ideal, the release of the positron does not have a sharp edge in time.

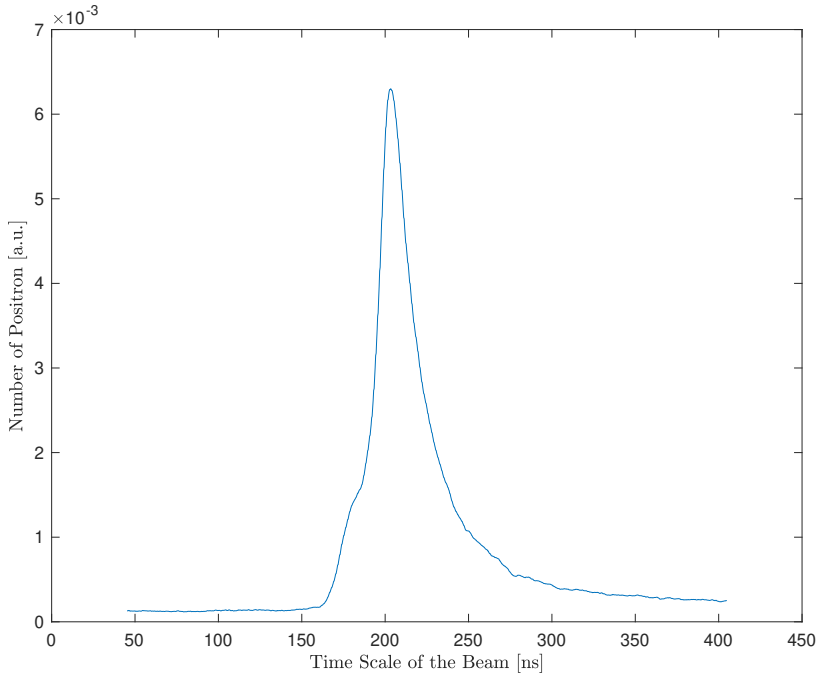

Figure 4.1: Measured time distribution of the beam

Fig. 4.2 shows the measured time and energy distribution of positrons and it is inputed as the initial condition for this simulation, which made by combining energy distribution (fig. 3.2) with time distribution (fig. 4.1)

The positrons get bunched when they exit the buncher and fly through a long tube with ground potential but a forward magnetic to constrain their motion

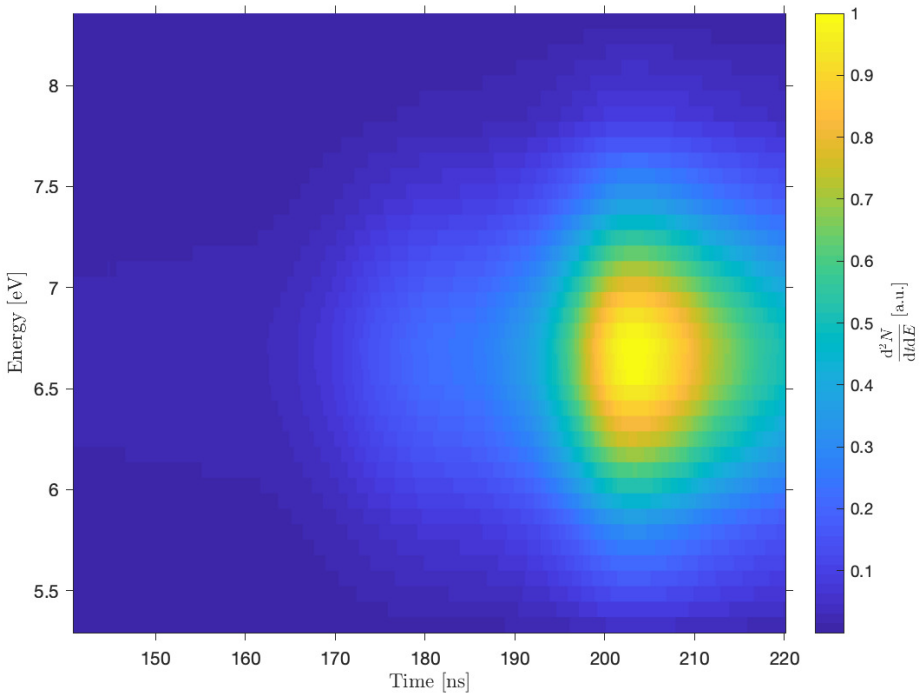

Figure 4.2: Real time and energy distribution inputed

perpendicular to the tube. Then, the positrons reach the elevator, in which the potential is raised to 6 kV to assure their energy to be high enough for hitting the target.

In Fig. 4.3, the energy is first reduced at the entry of the buncher by a voltage offset of the buncher, because only with reduced energy can positrons have low enough velocity to fit in the buncher so that the last one enters before the first one exits.

In Fig. 4.4, we can see the energy of the positrons was reduced by the voltage offset of the buncher. The bottom figure demonstrates that the positrons leaving at latter time will have a higher energy which matches our expectation.

In Fig. 4.5, the same logic was applied to the elevator to assure the positron beam can fit in the elevator. The voltage is risen to 6 kV for the positrons to have high enough energy to strike the target. As shown in Fig. 4.5, the energy of positrons is risen by 6 keV, and the time scale indicates the time of arrival and leaving the elevator. After the elevator, the positrons hit the target in very short time because they speed is very high. Therefore, their time-energy distribution will be similar as the bottom one in Fig. 4.5.

In the end, we applied fit to the time distribution of the positrons at the

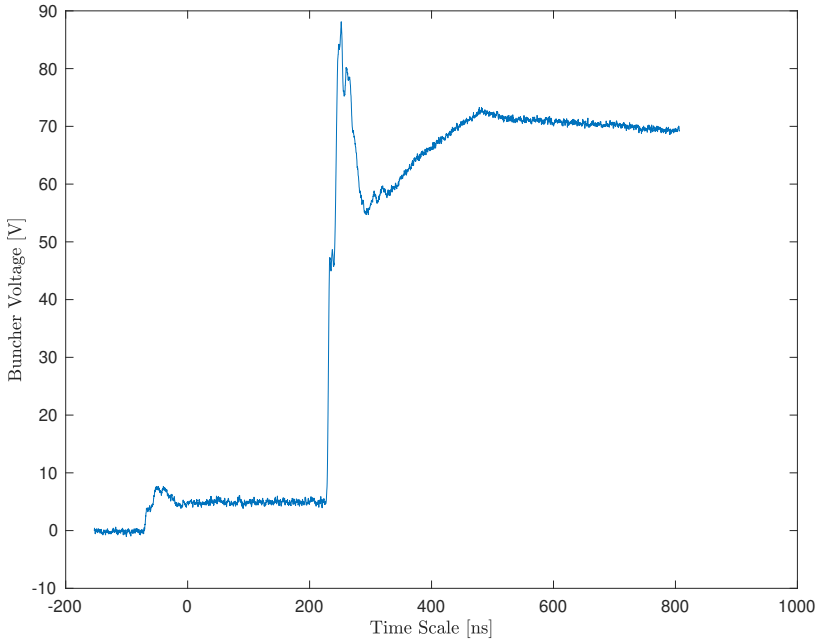

Figure 4.3: Measured real buncher waveform, generated according to the Eq. 4.1

target. The sigma of this shape in the Fig. 4.6 is 6.4, thus the FWHM of the arrival time is around 16.6 ns in simulation.

To note, the waveform of the elevator is improved. Before the rise time for the voltage from 0 to 6 keV was more than 200 ns but is now improved to be around 20 ns. This is done by shorten the cable length between the high-voltage amplifier and the elevator, as the cable is shielded that has very high capacitance per meter. With the fast rise time, the elevator is able to bunch the positrons even when they are accelerated by the buncher with energy of around 100 eV, which gives us more voltage space to adjust the buncher waveform.

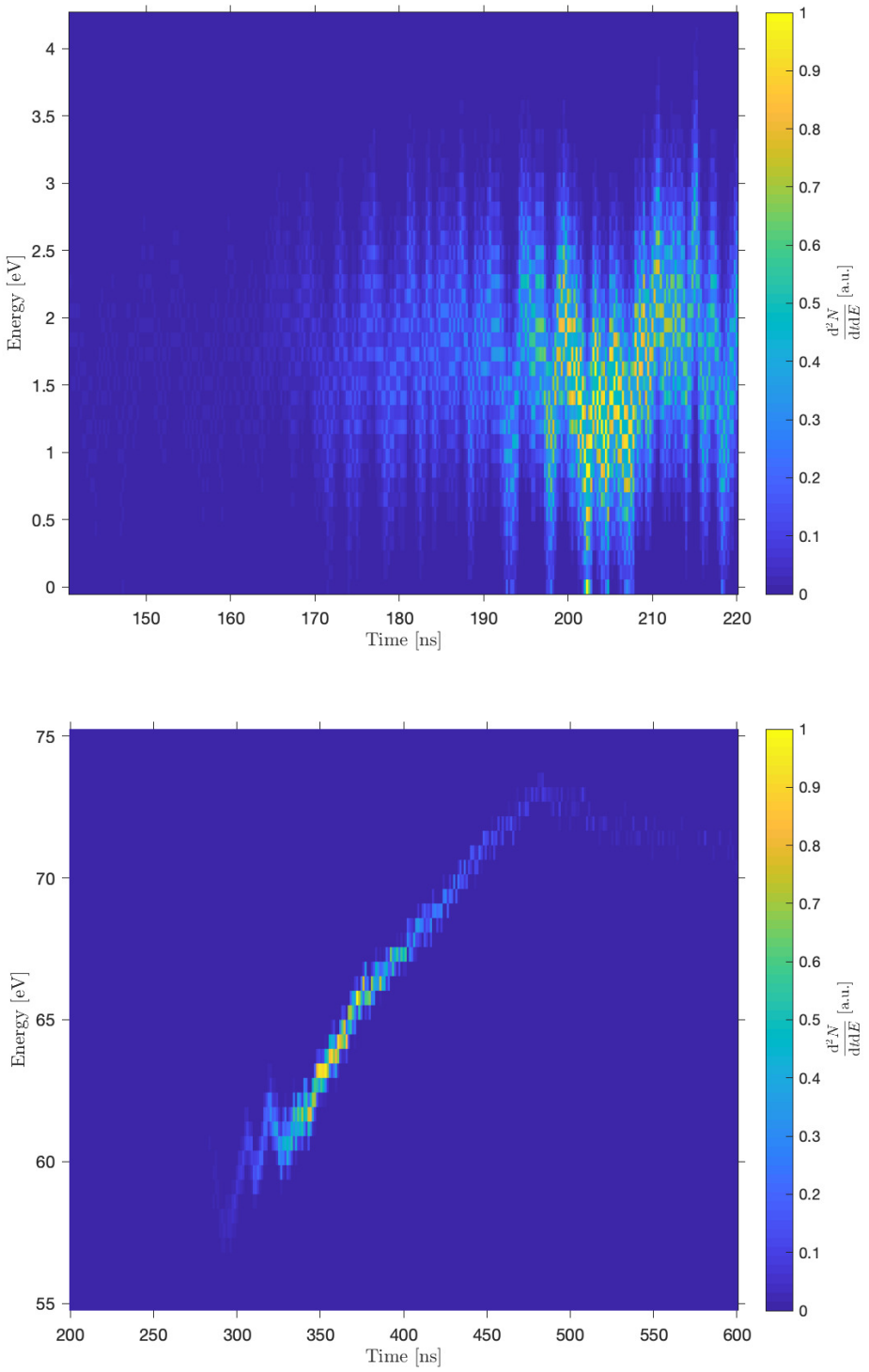

Figure 4.4: Simulated time and energy distribution at the entry of buncher (up) and at the exit of buncher (down)

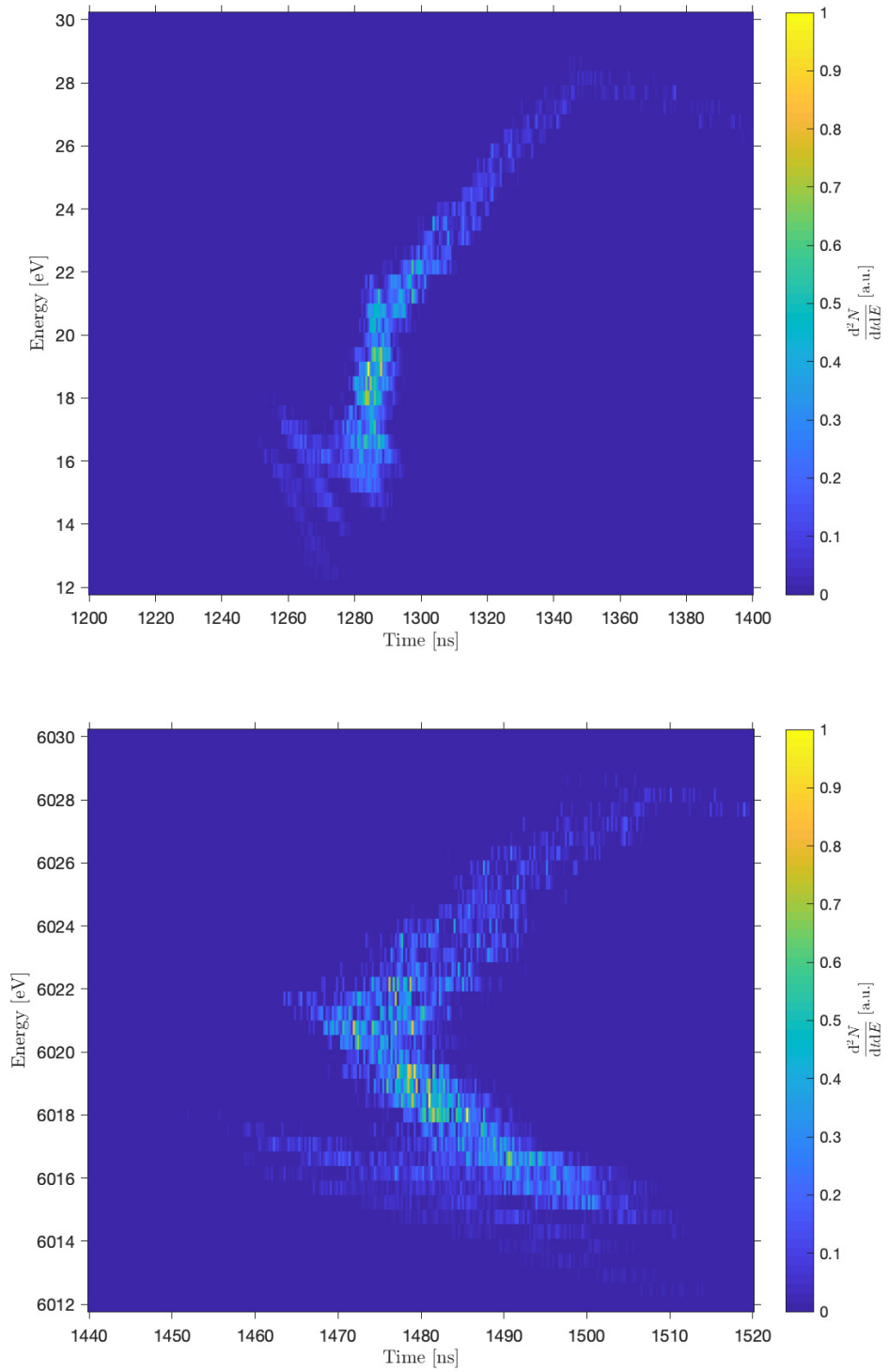

Figure 4.5: Simulated time and energy distribution at the entry of elevator (up) and at the exit of elevator (down).

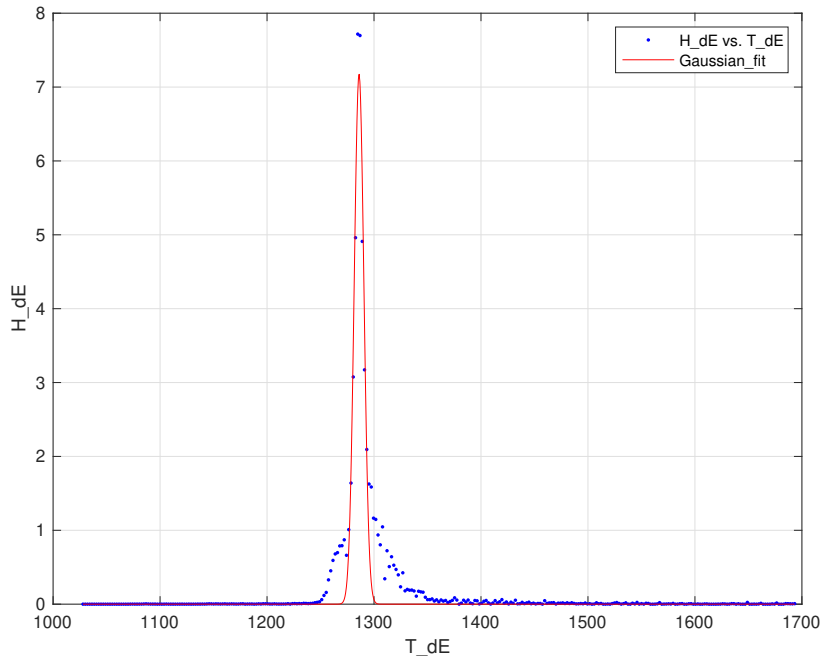

Figure 4.6: The number of positrons arrive at the target vs time

Chapter 5

Laser system

A fine-tuning laser centered at 486 nm wavelength is implemented for exciting the positrons to from 1s to 2s state. The laser system consists of a Toptica frequency stabilized CW laser, which corresponds to half the frequency of the transition. Since the CW laser alone cannot excite the 1s to 2s efficiently, an additional Radiant Dyes pulsed dye amplifier is used, which is pumped by a Spectra Physics pulsed Nd:YAG operating in the UV. Given the natural linewidth is around 1.2 MHz, the laser can be detuned for a few hundreds of MHz to generate the line shape and find the central position. This system is able to deliver about 20 mJ energy for a single pulse of 7 ns.

Chapter 6

Data analysis and results

The timed data for each single pulse was taken from the MCP, the scintillator and two laser diodes. Since the MCP was only connect to a single cathode, there is no spatial resolution for the annihilated photons. The diodes are the indicators for the lasers' states. For example, if the blue one is on, the signal of o-Ps is expected. If not, the background without excitation should be recorded. The MCP data is used for searching potential signal. For each laser frequency, events are combined to form a histogram of time and number of spikes. The background was accumulated for a large amount of events and then normalized to the events number of data for each frequency. The background shape is subtract from the signal+background data.

6.1 Processing of raw data

For each release of the positrons, the MCP voltage reading is recorded with respect to time. Then, the peaks in the MCP reading are marked as the decay signal of 2s and the time point of these "signal" are extracted. There are two ways to do detect peaks; one is to regard everything above certain threshold voltage as "signal", i.e., we can count more "signals" in wider peaks, while narrower peak has less "signals". This algorithm is most degraded around the "big peak", where most 1s positrons scatter from the target arrive at the MCP. Another, and is an improved algorithm is used to eliminate the multi-counting effect and increase the sensitivity of the "big peak" time interval. We detect local maximum of the MCP reading as peaks, thus width of the peaks has no effect on the number of "signal" we count. Besides, the minimum time separation of the peaks can be adjusted to assure the power to reject random noise. An example of a single beam is shown in Fig. 6.1.

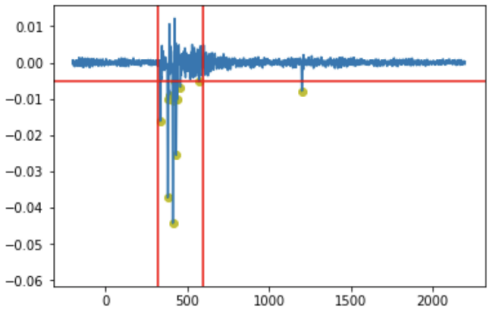

Figure 6.1: Peak detection example for a single time MCP reading voltage (V) vs time (ns). Horizontal red line is the threshold. Vertical red lines are the time interval of most scattered 1S detected. Dots indicates the detected peaks.

6.2 Improvement from implementation of the buncher

As the buncher introduced in chapter 4 can shorten the arrival time window of the positrons at the target, the MCP reading of scatter positrons should have a narrower peak. Although the MCP is tilted, the shape of the arrival does show a significant improvement, shown in Fig. 6.2. The fit of an exponential function is added to roughly show the τ the decay time.

It is clear that the decay time of the graph of bunched beam is lesser in Tab. 6.1. Also, the systematic error for different measured data-set is checked to be not comparable larger than the given statistical error, and here it is ignored because these data-set are just too scarce and does not reflect true variance within group.

τ_{old} (s^{-1})	τ_{new} (s^{-1})
0.01254 ± 0.00034	0.00757 ± 0.00020

Table 6.1: The exponential fit value to two background shapes, standard deviation is given for statistical error.

6.3 Signal significance

The background-only data sets are collected under the condition that either the blue laser is off or the laser frequency is far off resonance. Event is defined as a single release of positrons as shown in Fig. 6.1. The new background-only data set contains total of 3004 events, which includes 9924 peaks, roughly 3.3 peaks per event. We run the same procedure to collect signal data set except the

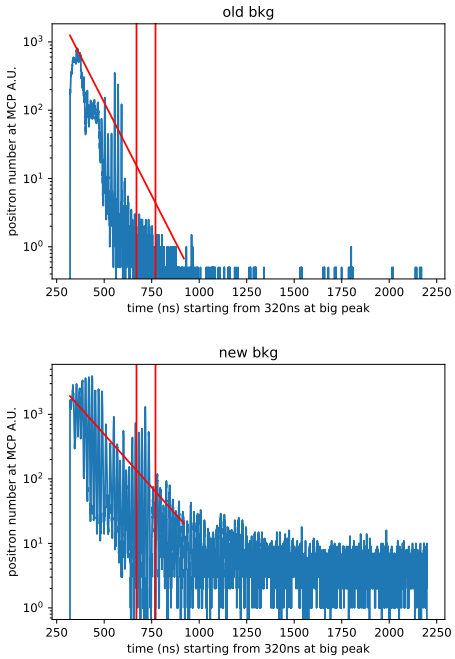

Figure 6.2: The MCP reading of w/o bunching and w/ bunching when laser is off. Vertical lines are for the time window of interest (expected 2S decay). A fit is also added.

blue laser is on. Different frequencies are collected separately. Then, histogram of signal data sets are normalized to the number events w.r.t background-only. Four different frequencies are plotted. We integral the histograms of prominent time interval. The expect decay of 2S observed is 0.02-0.2 per event, resulting 60-600 events in that integrated interval.

The results are plotted in Fig 6.3 with signal events counts. The counts is the final result that shows the number of 2s of the laser excitation at the given frequency.

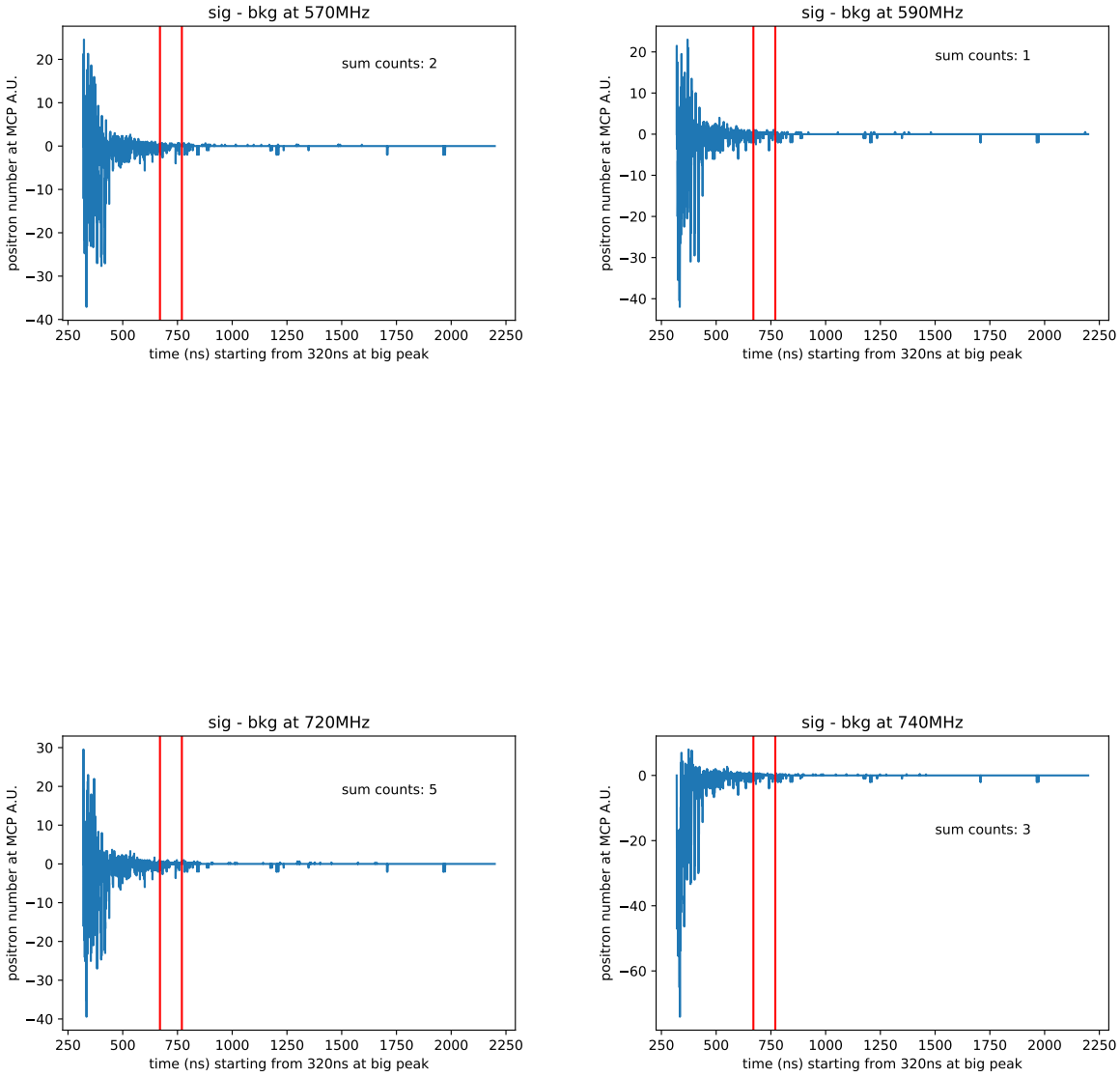

Figure 6.3: Histograms of signal happen time with red laser on (sig) minus that of red laser off (bkg). Red window is the probable signal period. The counts is the surplus of sig data set compare to bkg data set in red window.

Bibliography

[1] M. S. Fee et al., Phys. Rev. A **48**, 192 (1993).

[2] M. Haas et al., Phys. Rev. A **73**, 052501 (2006).

[3] M. W. Heiss, G. Wichmann, A. Rubbia, and P. Crivelli, Journal of Physics: Conference Series **1138**, 012007 (2018).

[4] M. Deutsch, Phys. Rev. **82**, 455 (1951).

[5] P. J. Mohr, B. N. Taylor, and D. B. Newell, Journal of Physical and Chemical Reference Data **41**, 043109 (2012).

[6] C. G. Parthey et al., Phys. Rev. Lett. **107**, 203001 (2011).

[7] S. Chu, A. P. Mills, and J. L. Hall, Phys. Rev. Lett. **52**, 1689 (1984).

[8] W. Demtröder, *Laser Spectroscopy: Vol. 1: Basic Principles*, Springer Science and Business Media, 4, illustrated edition, 2008.

[9] L. Gerchow et al., Instruments **2** (2018).

[10] C. Surko, *Accumulation, storage and manipulation of large numbers of positrons in traps I — The basics*, pages 83–128, 2014.

[11] C. Vigo, Search for invisible decay channels of positronium confined in a vacuum cavity, 2017.

[12] D. A. Cooke et al., Journal of Physics B: Atomic, Molecular and Optical Physics **49**, 014001 (2015).

Appendix A

Outlook for buncher improvement

Assuming the energy distribution in each time frame within the opening time are the same, the positrons fly from the gate to the entry of buncher will spread out a little to be more than 50 ns because the ones with higher energy at the front of the beam will has higher velocity thus move further away from the center of the beam while lasted ones with lower energy will be slower and also move away from the center of the beam. This effect is proportional to the flying time and eventually will "sort" these positrons in such way that higher energy one come first and lower energy come last also, the energy spread in a particular time frame will become much less than the initial released one, as predicted and shown in Fig.A.1.
With this effect taking into account, a slight adjustment of the buncher waveform (Fig.4.3) can improve the buncher performance to its best.

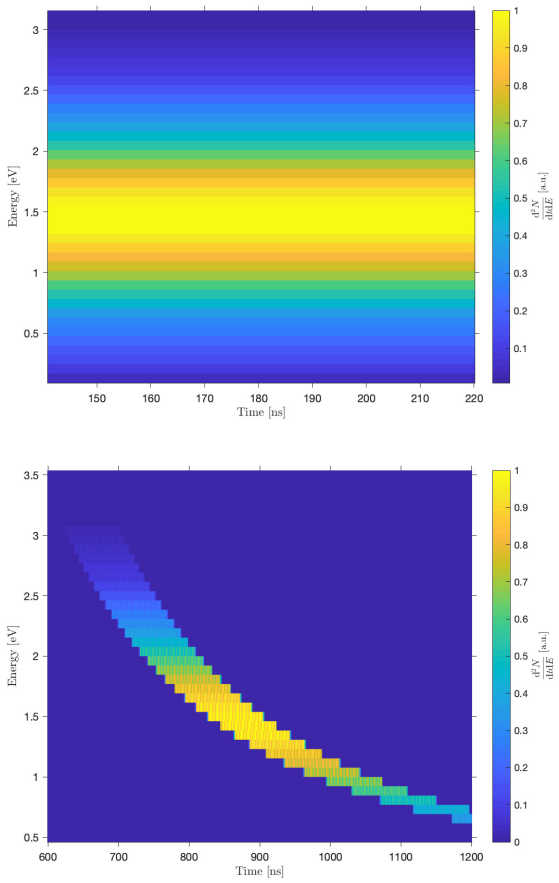

Figure A.1: Time spread out after 0.5 m of flying with real energy distribution but lower mean energy